Numerical Calculation of Turbulent Open-Channel Flows in Consideration of Free-Surface Effect

AUTHOR(S):

NEZU, Iehisa; NAKAGAWA, Hiroji

Mem. Fac. Eng., Kyoto Univ. Vol. 49, No. 2 (1987)

Numerical Calculation of Turbulent Open-Channel Flows in Consideration of Free-Surface Effect

by

Iehisa NEZU* and Hiroji NAKAGAWA*

(Received December 12, 1986)

Abstract

Numerical calculation techniques of turbulent shear flows are classified into two categories: one is the k-ε turbulence model, and the other is the large eddy simulation (LES). The standard k-ε model has been established at present to predict a turbulent structure in jets, boundary layers and closed channel flows, while LES is being developed to predict a coherent eddy structure in simpler channel flows. The standard k-ε model cannot be, however, easily applied to open channel surface flows, because the turbulence near the free surface is more depressed than the closed channel flows.

In the present study, a new modified k-ε model is proposed to predict reasonably a turbulent structure in open channel flows with both the low and high Reynolds numbers. The numerical calculations indicate a good agreement with the experimental data which were obtained by making use of hot-film and Laser Doppler anemometers.

1. Introduction

Numerical calculation techniques of turbulent shear flows are classified into two categories: one is the multi-equation model of turbulence, and the other is the large-eddy simulation. The large-eddy simulation (LES) stems from an idea in which the larger scale turbulence rather than the calculating grid (resolvable scale) is calculated in time-dependent Navier-Stokes equations that incorporate the local-isotropic turbulence model for a small-scale turbulence (subgrid scale). The first application of LES was made by Deardorff (1970), who simulated a closed channel flow at a large Reynolds number. Using this LES technique, Moin & Kim (1982) could successfully simulate the bursting phenomena near the wall which were intensively investigated experimentally in the 1970's by many

* Department of Civil Engineering, Kyoto University, Kyoto 606, Japan.

researchers. (See reviews written by Hinze (1975), Laufer (1975), Willmarth (1975), Nakagawa & Nezu (1981) and Cantwell (1981)). The LES is an epoch-making computer simulation of wall turbulence which can predict the coherent structure of turbulent shear flows. However, it takes a very large computational time, that is, even the computation of simple flows such as uniform closed channel flows needs several hours of the CPU-time in the newest super-computer (e. g. Kobayashi et al. 1985, 86). Hence, LES does not yet, at present, attain an engineering prediction technique for fluid flow and heat-mass transfer.

On the other hand, the multi-equation model of turbulence was developed and tested intensively by the Imperial College group in the 1970's. This multi-equation model solves the Reynolds equations on the basis of the turbulent eddy-viscosity model. In a previous simpler model, such as the mixing-length model, the eddy viscosity had to be given as a known variable. However, in the multi-equation model the eddy viscosity is an unknown variable, and it is solved by using the transport equation of turbulence. The k-ε model is the most representative one of the multi-equation models. The k-ε model can predict fairly reasonably and cost-performably a turbulent structure and heat-mass transfer in jets, boundary layers, closed channel flows and, furthermore, complex turbulent flows. (See a review written by Rodi (1980)). Consequently, the model constants in the k-ε model have been, at present, established as standard values, i. e. the standard k-ε model (Rodi, 1980).

In the early 1980's, the Rodi group in the University of Karlsruhe began to apply the k-ε model to the hydraulic problems (Rodi 1980). In the application to open-channel flows, the effects of free surface on turbulence must be considered reasonably. Naot & Rodi (1982) proposed an algebraic-stress version of the k-ε model by taking into account the damping effect of the turbulence near the free surface which was pointed out by Nakagawa, Nezu & Ueda (1975) and they predicted the secondary currents in open-channel flows. The validity of this prediction was then verified experimentally by Nezu & Rodi (1985), who carried out highly accurate measurements by making use of Laser Doppler anemometers (See Rodi (1986)). Recently, Celik & Rodi (1984) refined the algebraic-stress version of the k-ε model, and made a calculation of two-dimensional open-channel flows. However, 5 new constants were further necessary in their model, in addition to the standard constants of the k-ε model. The coefficient C_μ of the eddy viscosity indicated also a very large variation in comparison with the closed channel flows, as will be shown later. Therefore, it is necessary to develop a more reasonable numerical calculation model of turbulent open-channel flows.

The present study proposes a new modified k-ϵ model in which the damping effect of the turbulence near the free surface is considered by introducing the damping factor. The present model can predict reasonably a turbulent structure of open-channel flows at large Reynolds numbers. Furthermore, when the Reynolds number is low, the present model can be extended easily by introducing the extra terms of Jones & Launder (1973). The present calculation results indicate a good agreement with the experimental ones at both low and high Reynolds numbers.

2. Basic Equations

2.1 Reynolds Equations

The Reynolds equations and continuity equation in two-dimensional (2-D) open-channel flows are given as follows:

$$U\frac{\partial U}{\partial x}+V\frac{\partial U}{\partial y}=g\sin\theta-\frac{\partial}{\partial x}\left(\frac{P}{\rho}\right)+\frac{\partial}{\partial x}\left(-\overline{u^2}\right)+\frac{\partial}{\partial y}\left(-\overline{uv}\right)+\nu\nabla^2U \tag{1}$$

$$U\frac{\partial V}{\partial x}+V\frac{\partial V}{\partial y}=-g\cos\theta-\frac{\partial}{\partial y}\left(\frac{P}{\rho}\right)+\frac{\partial}{\partial x}\left(-\overline{uv}\right)+\frac{\partial}{\partial y}\left(-\overline{v^2}\right)+\nu\nabla^2V \tag{2}$$

$$\frac{\partial U}{\partial x}+\frac{\partial V}{\partial y}=0 \tag{3}$$

The x co-ordinate is aligned with the streamwise direction. The co-ordinate y is perpendicular to the channel wall, and z is in the spanwise direction. The mean velocities in the x, y and z directions are U, V and W ($\equiv 0$), and their turbulent fluctuations are u, v and w, respectively. P is the mean pressure, ρ is the water density, g is the gravity acceleration, ν is the kinematic viscosity and θ is the channel slope. The first terms on the right-hand side of (1) and (2) describe the gravity force acting on the water flow.

Denoting the pressure deviation P' from the hydrostatic pressure, i. e.

$$P\equiv\rho g(h-y)\cos\theta+P' \tag{4},$$

the gravity term is dropped out of (2), where h is the water depth of open-channel flow. To close Equations (1) and (2), the Reynolds stresses $\overline{u^2}$, $\overline{v^2}$ and

$-\overline{uv}$ must be correlated with the mean velocities U and V. This closure problem is the most essential but difficult one in turbulence research. The representative examples of the closure problem are the eddy-viscosity model (Boussinesq 1877) and the mixing-length model (Prandtl 1925).

2.2 Turbulent Eddy-Viscosity Model

The turbulent eddy-viscosity model of Boussinesq (1877) has been re-examined and refined on the basis of the modern turbulence similarity law (e. g. Rotta (1972) and Townsend (1976)). As a result, the following relations are satisfied:

$$\overline{u_i u_j} = -\nu_t\left(\frac{\partial U_i}{\partial x_j} + \frac{\partial U_j}{\partial x_i}\right) + \frac{2}{3} k\,\delta_{ij} \tag{5}$$

$$\nu_t \equiv C_\mu k^2/\varepsilon \tag{6}$$

$$k \equiv \frac{1}{2}\overline{u_i u_i} = \frac{1}{2}\left(\overline{u^2} + \overline{v^2} + \overline{w^2}\right) \tag{7}$$

where, ν_t is the eddy viscosity and δ_{ij} is the Kronecker delta. k is the kinetic turbulent energy, while ε is its turbulent dissipation. In the previous eddy-viscosity model, ν_t had to be given beforehand as a known variable, which was very difficult except for only simple flows such as the uniform pipe flow.

On the other hand, the turbulence similarity law verifies the relation of (6). Although C_μ is the empirical coefficient, both k and ε are the most important quantities in turbulent structures. The closure problem in which k and ε are chosen as unknown variables in the equations is the so-called k-ε turbulence model.

2.3 k-equation and ε-equation

(1) k-equation

The turbulent energy equation is exactly reduced to

$$U\frac{\partial k}{\partial x} + V\frac{\partial k}{\partial y} = G - \varepsilon - \frac{\partial}{\partial x}\left(\frac{\overline{pu}}{\rho} + \overline{ku} - \nu\frac{\partial k}{\partial x}\right) - \frac{\partial}{\partial y}\left(\frac{\overline{pv}}{\rho} + \overline{kv} - \nu\frac{\partial k}{\partial y}\right) \tag{8}$$

$$G \equiv -\overline{u_i u_j}\frac{\partial U_i}{\partial x_j} \tag{9}$$

where, p is the pressure fluctuation, and G is the generation or production of the

turbulent energy. The third and fourth terms of (8) are the turbulent diffusion which describes the third-order correlations. In order to close Equation (8), the diffusion terms must be approximated by the second-order correlations. In the same conception as (5), the following gradient-type relation is valid:

$$\overline{\left(\frac{p}{\rho}+k\right)u_i} \equiv -\frac{\nu_t}{\sigma_k}\frac{\partial k}{\partial x_i} \tag{10}$$

where, σ_k is the model constant.

The diffusions of kinetic energy k and pressure energy p/ρ are identified overall in the model of (10). However, because both of them are quite different from each other very near the wall (e. g. Laufer (1954) and Nezu (1977)), (10) cannot be applied to the viscous sublayer. Paying attention to $k \propto y^2$ very near the wall, Jones & Launder (1973) proposed an extra term D to (10) :

$$D \equiv C_3\,\nu\left(\frac{\partial\sqrt{k}}{\partial y}\right)^2 \tag{11}$$

where, C_3 is the model constant of about 2.

(2) ε-equation

The energy dissipation ε is defined as

$$\varepsilon \equiv \nu\overline{\left(\frac{\partial u_j}{\partial x_i}\right)\left(\frac{\partial u_i}{\partial x_j}\right)} \tag{12}$$

The ε-equation can be induced from the Navier-Stokes equation, but it is much more complicated than (8). (See Hanjalic & Launder (1976).) Hence, the same -type relation as (8) is assumed in the following:

$$U\frac{\partial\varepsilon}{\partial x}+V\frac{\partial\varepsilon}{\partial y}=\frac{\varepsilon}{k}\left(C_1G-C_2\varepsilon\right)+\frac{\partial}{\partial x}\left(\frac{\nu_t}{\sigma_\varepsilon}\frac{\partial\varepsilon}{\partial x}\right)+\frac{\partial}{\partial y}\left(\frac{\nu_t}{\sigma_\varepsilon}\frac{\partial\varepsilon}{\partial y}\right) \tag{13}$$

where, C_1, C_2 and σ_ε are the model constants.

Although (13) may be an empirical equation, it can predict turbulence more reasonably than the previous simple model (e. g. Rodi (1980)). For the same reason as the k-equation, an extra term E is necessary very near the wall. In the Jones & Launder model (1973), E is given by

$$E \equiv C_4\,\nu\,\nu_t\left(\frac{\partial^2 U}{\partial y^2}\right)^2 \tag{14}$$

where, C_4 is the model constant of about 2.

2.4 General Description of Basic Equations

5 partial differential equations of (1), (2), (3), (8) and (13) are reduced to the same-type transport equation:

$$\frac{\partial}{\partial x}\left(\phi U - \Gamma\frac{\partial\phi}{\partial x}\right)+\frac{\partial}{\partial y}\left(\phi V - \Gamma\frac{\partial\phi}{\partial y}\right)=S_\phi \tag{15}$$

ϕ is the transported variable and S_ϕ is its source term. Γ is the effective viscosity. (15) reads as follows:

$$\text{Continuity equation: } \phi = 1,\ S_\phi = 0 \tag{16}$$

U-equation: $\phi = U,\ \Gamma = \nu_t + \nu$

$$S_u = g\left(\sin\theta - \frac{dh}{dx}\cos\theta\right)-\frac{\partial}{\partial x}\left(\frac{P'}{\rho}\right) + \frac{\partial}{\partial x}\left(\Gamma\frac{\partial U}{\partial x}\right)+\frac{\partial}{\partial y}\left(\Gamma\frac{\partial V}{\partial x}\right) \tag{17}$$

V-equation: $\phi = V,\ \Gamma = \nu_t + \nu$

$$S_v = -\frac{\partial}{\partial y}\left(\frac{P'}{\rho}\right)+\frac{\partial}{\partial x}\left(\Gamma\frac{\partial U}{\partial y}\right)+\frac{\partial}{\partial y}\left(\Gamma\frac{\partial V}{\partial y}\right) \tag{18}$$

k-equation: $\phi = k,\ \Gamma = \nu_t/\sigma_k$

$$S_k = G - (\varepsilon + D) \tag{19}$$

ε-equation: $\phi = \varepsilon,\ \Gamma = \nu_t/\sigma_\varepsilon$

$$S_\varepsilon = \frac{\varepsilon}{k}\left(C_1 G - C_2\varepsilon\right) + E \tag{20}$$

The turbulent generation G is obtained from (5) and (9), as follows:

$$G = \nu_t\left(2\left(\frac{\partial U}{\partial x}\right)^2 + 2\left(\frac{\partial V}{\partial y}\right)^2 +\left(\frac{\partial U}{\partial y}+\frac{\partial V}{\partial x}\right)^2\right) \tag{21}$$

When the extra terms D and E are introduced to (19) and (20), the boundary condition can be determined so that $k=\varepsilon=0$ at $y=0$.

3. Standard k-ε Model and Its Limitation of Application

3.1 Model Constant

The Imperial College group found, through intensive investigation and computational optimization, that the standard k-ε model of (15) could be applied to jets, boundary layers and closed channel flows. Consequently, they proposed the following standard model constants (See Rodi (1980).):

$$\sigma_k = 1.0,\ \sigma_\varepsilon = 1.3,\ C_1 = 1.44 \text{ and } C_2 = 1.92 \tag{22}$$

In the k-ε model, the coefficient of C_μ of (6) is the most important parameter. When the Reynolds number becomes sufficiently large, C_μ can be regarded as a universal constant (Townsend (1976)). Its standard value is given as follows (Rodi (1980)):

$$C_\mu = 0.09 \tag{23}$$

3.2 Boundary Conditions

(1) Wall condition (wall function)

As mentioned previously, the gradient-type description of diffusion such as (10) cannot be applicable up to the wall, i. e. $y = 0$. In order to circumvent this difficulty, the standard k-ε model assumes that, when $y^+ \equiv yU_*/\nu$ (where, U_* = friction velocity) becomes larger than 50, the turbulent structure attains an energy equilibrium, i. e. $G \cong \varepsilon$, and also the log law distribution is satisfied there.

Denoting the first grid point nearest the wall as y_p (the value corresponding to y_p is denoted by the suffix p.), the following boundary condition, i. e. wall function, is obtained from the above-mentioned assumption.

(i) Mean velocity: $$U_p/U_* = \frac{1}{\kappa} \ln y_p^+ + A \tag{24}$$

where, the empirical values of κ and A are given as $\kappa = 0.41$ and $A = 5.3$ in open-channel flow (Nezu & Rodi (1986)).

(ii) Because $G = \varepsilon$ for $y_p^+ \geq 50$ (25),

the following relation can be obtained:

$$k_p / U_*^2 = 1/\sqrt{C_\mu} = 3.33 \tag{26}$$

$$\varepsilon_p = \frac{U_*^3}{\kappa y_p} \tag{27}$$

(2) Symmetrical condition

Since the flow should be symmetric on the central axis, i. e. $y=h$, in the case of closed channel flows, the following symmetrical condition is satisfied:

$$\frac{\partial U}{\partial y}\Big|_{y=h} = 0, \quad \frac{\partial k}{\partial y}\Big|_{y=h} = 0, \quad \frac{\partial \varepsilon}{\partial y}\Big|_{y=h} = 0 \tag{28}$$

3.3 Limitation of Application of Standard k–ε Model

The closed channel flow can be numerically calculated by solving the equations of (15) on the boundary conditions of (24), (26), (27) and (28). However, the standard k–ε model has the following inevitable limitations of application:

(i) The Reynolds number Re should be set sufficiently large, and thus $y_p^+ > 50$ must be satisfied. Then, the turbulent energy k_p keeps constant as $k_p / U_*^2 = 3.33$, irrespective of flow conditions.

(ii) The symmetrical condition of (28) is not applicable to open-channel flows, because the effect of free surface appears.

(iii) Because (5) is premised on an isotropic flow, the standard k–ε model cannot be applicable to phenomena which are driven by anisotropy of turbulence. For example, the secondary currents in duct flows cannot be calculated by using the standard k–ε model.

The limitation of (i) is a fatal shortcoming as the Reynolds number becomes lower. In this case, the extra terms of D and E may be useful to predict a turbulence near the wall. The present study proposes a new wall function whereby the first grid point y_p can be extended up to $y_p^+ = 20$. Furthermore, when the Reynolds number is comparatively small, the validity of D and E is examined in open-channel flows.

The limitation of (ii) is the most inevitable defect for the numerical calculation of open-channel flows. That is to say, the modelling of the effect of the free surface is the most important topic in the application of the k–ε model to hydraulics. Assuming the equilibrium condition of $G = \varepsilon$ in the transport equation of $\overline{u_i u_j}$, Celik & Rodi (1984) proposed an algebraic-stress version of the k–ε model, as follows:

$$\frac{\overline{v^2}}{k} = \frac{2}{3}\frac{R_1 - 1 + (G/\varepsilon)(R_2 - 2R_2R_4f)}{R_1 + (G/\varepsilon) - 1 + 2R_3f} \tag{29}$$

$$C_\mu = 0.09 \frac{1+\frac{3}{2}\frac{R_2 R_4 f}{1-R_2}}{1+\frac{3}{2}\frac{R_3}{R_1} f} \cdot \frac{1-\frac{2R_2R_4f\ (G/\varepsilon)}{R_1-1+R_2\ (G/\varepsilon)}}{1+\frac{2R_3 f}{R_1-1+G/\varepsilon}} \tag{30}$$

where, R_1, R_2, R_3 and R_4 are model constants. Celik & Rodi used $R_1 = 1.8$, $R_2 = 0.6$, $R_3 = 0.5$, $R_4 = 0.3$ which were given by Gibson & Launder (1978). Also, f is a wall function. They determined f so that the vertical turbulence intensity $\overline{v^2}$ of (29) might coincide with the experimental values obtained by Nakagawa, Nezu & Ueda (1975). In the Celik & Rodi model, 5 new model constants of $R_1 - R_4$ and f have to be given, in addition to the standard constants of (22). Furthermore, Celik & Rodi used a free-surface condition which was proposed by Hossain (1980), that is,

$$\varepsilon_s h / U_*^3 = \frac{C_\mu^{3/4}}{0.07\kappa} (k_s / U_*^2)^{3/2} = \frac{1}{0.18} (k_s / U_*^2)^{3/2} \tag{31}$$

where, suffix s denotes the value at the free-surface. However, (31) overestimates the dissipation much more than the experimental values. According to Nezu (1977), k_s / U_*^2 is nearly equal to 0.85. Then, (31) estimates $\varepsilon_s h / U_*^3 = 4.4$, which is much larger than the experimental values, as will be shown later. Consequently, the algebraic-stress model of Celik & Rodi should be refined further.

Lastly, the limitation of (iii) is important to predict three-dimensional turbulent flows such as secondary currents. Although the anisotropic k-ε model has been recently proposed by some researchers (e. g. Nakayama, Chow & Sharma (1983)), sufficient models may be not available yet. Such a development of the 3-D computation technique will be further necessary.

4. A New Modified k-ε Model

4.1 Scope of the Present Modified k-ε Model

As mentioned in Chapter 3, the standard k-ε model has some substantial shortcomings in application to open-channel flows. The present study proposes a new modified k-ε model to circumvent these difficulties. However, considering that the standard k-ε model is recognized to be a very powerful computation technique in fluid engineering (e. g. Gosman, Launder & Reece (1985)), its model should be extended straightforward so as to be valid even in open-channel flows. The present extensions of the standard k-ε model are as follows:

(i) The coefficient C_μ which is the most essential parameter in the k-ε model should be influenced by the viscous effect, so as to extend the first grid point y_p^+ up to 20.

(ii) The damping effect of turbulence should be considered in modelling the free surface condition.

(iii) The new model can also predict a turbulent structure at a low Reynolds number and, furthermore, in viscous sublayer even at a high Reynolds number.

These extensions are formulated in order in the following sections.

4.2 Coefficient C_μ of Eddy-Viscosity Model

In the same way that van Driest (1956) formulated the damping function near the wall in the mixing-length model, a damping function should be introduced into the coefficient C_μ to extend the eddy-viscosity model up to the viscous sublayer. The van Driest-type damping function is given by

$$C_\mu = 0.09\ (1 - D_1 \cdot \exp(-R_t / D_2)) \tag{32}$$

On the other hand, Jones & Launder (1973) proposed an empirical relation, as follows:

$$C_\mu = 0.09 \exp\left(\frac{-D_3}{R_t + D_4}\right) \tag{33}$$

where, $D_1 \sim D_4$ are the model constants which should be determined by comparison with the experimental results. Jones & Launder chose $D_3 = 125$ and $D_4 = 50$. $R_t \equiv k^2/(\nu\varepsilon)$ is the turbulence Reynolds number. In the same manner as van Driest's original idea, it may be possible to use y^+ instead of R_t in (32) and (33), but this case is not so relevant because C_μ depends directly on the grid point y^+. Of course, as the Reynolds number R_t becomes larger, (32) or (33) approaches $C_\mu = 0.09$, i.e. the standard model. The Celik & Rodi model of (30) may be also regarded as a kind of damping function.

Figure 1 shows the coefficient C_μ against the turbulence Reynolds number R_t, by choosing the model constants reasonably. Run 1 is the standard model ($C_\mu = 0.09$). Run 2 is the Jones & Launder type ($D_3 = 120$, $D_4 = 60$). Both Run 3 ($D_1 = 0.95$, $D_2 = 250$) and Run 4 ($D_1 = 0.90$, $D_2 = 200$) are the van Driest type. Although the van Driest type of (32) becomes nearly equal to the Jones & Launder type of (33) in the region of $R_t \leq 200$, the former approaches the standard model faster than the latter.

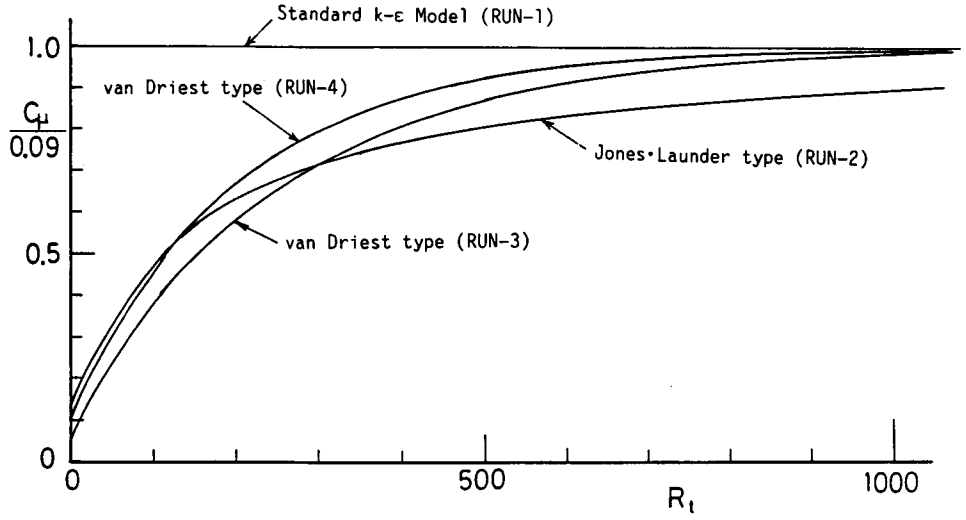

Figure 1. Coefficient C_μ of eddy viscosity against turbulence Reyonolds number, R_t.

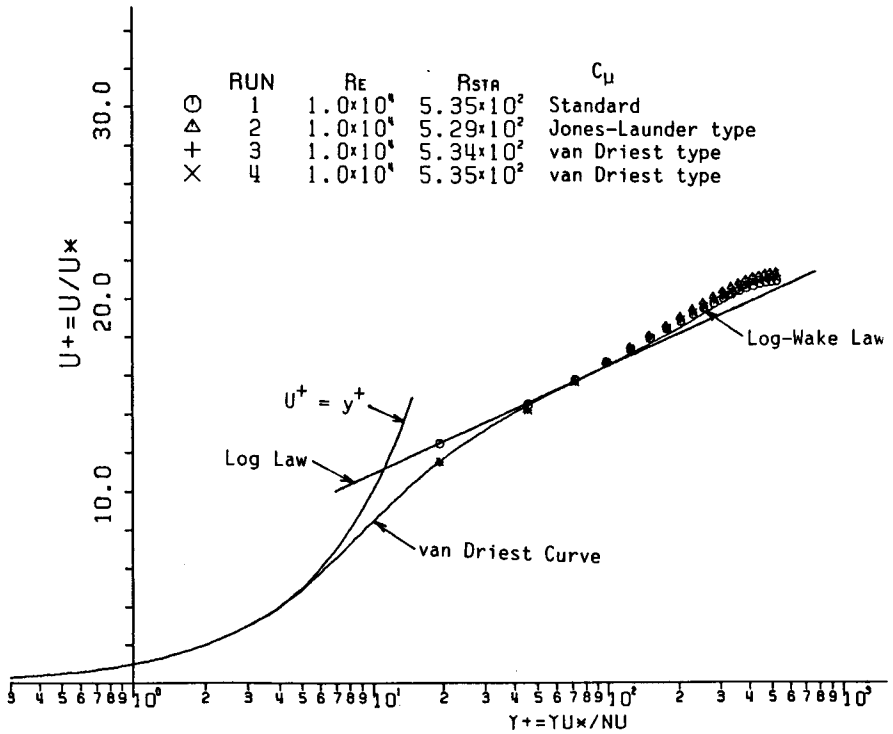

Figure 2 Effect of C_μ on mean velocity distribution (Standard k-ε model and modified k-ε model).

Figures 2, 3 and 4 are some examples of the calculation results to examine the effect of C_μ. A detailed computation technique will be mentioned later.

Firstly, Figure 2 shows the mean velocity distribution of $U^+ = U/U_*$ vs. $y^+ = yU_*/\nu$. This figure also shows the van Driest curve, the log law distribution of (24) and the log-wake law distribution which is described as

$$U^+ \equiv \frac{U}{U_*} = \frac{1}{\kappa} \ln y^+ + A + \frac{2\Pi}{\kappa} \sin^2\left(\frac{\pi}{2}\frac{y}{h}\right) \tag{34}$$

where, Π is the Coles' parameter. Nezu & Rodi (1986) recently found that Π should be equal to 0.2 in open-channel flows with a large Reynolds number. The curve of (34) with $\Pi = 0.2$ is shown in Figure 2. The standard model (Run 1) obeys, of course, the log law at y_p^+. This recognizes that the damping function should be used in the buffer layer. Among these runs, Run 3 indicates the best agreement with the log-wake law of (34).

Figure 3 shows the distribution of turbulent energy k/U_*^2. The calculated values include the damping effect of turbulence near the free surface, which will be discussed later. The solid line in Figure 3 is the semi-theoretical curve which was proposed by Nezu (1977), and it is given by

$$\frac{k}{U_*^2} = 4.78 \exp\left(-2 \cdot \frac{y}{h}\right) \tag{35}$$

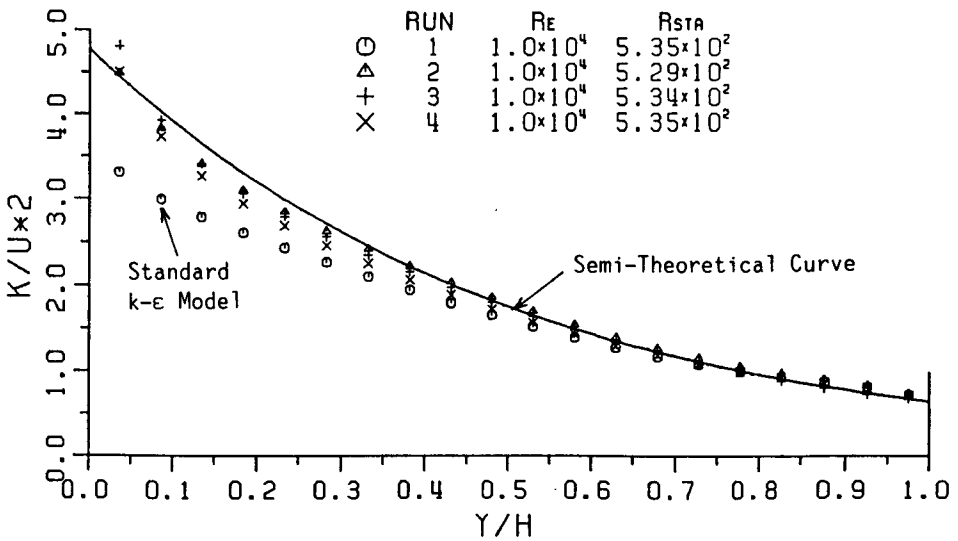

Figure 3. Effect of C_μ on turbulent energy, k/U_*^2.

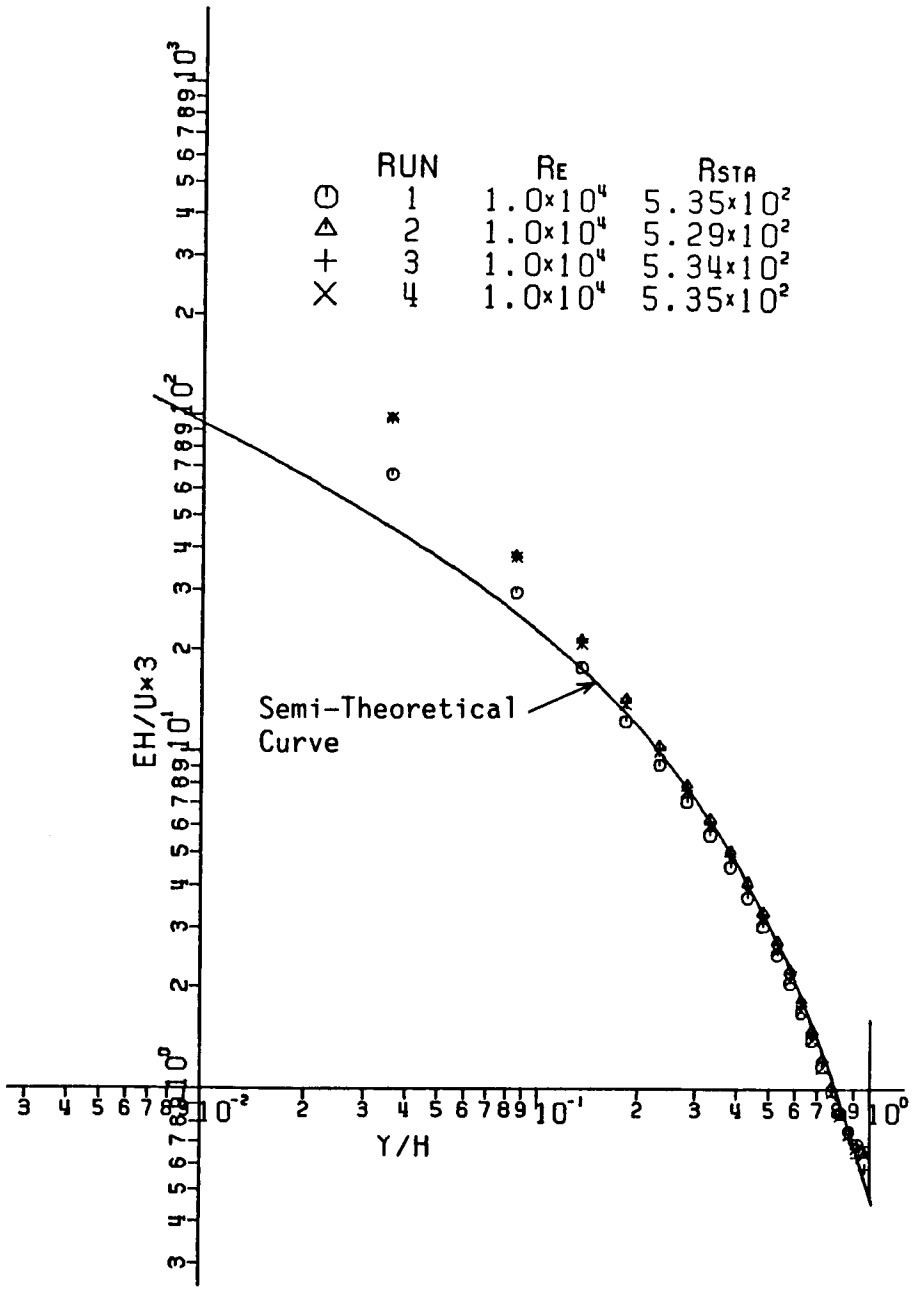

Figure 4. Effect of C_μ on energy dissipation, $\varepsilon h/U_*^3$.

(35) is valid in the outer region of $y/h > 0.15$ for open-channel flows. Figure 3 indicates clearly that the standard model (Run 1) deviates fairly largely from (35). Run 3 indicates the best agreement with (35).

Figure 4 shows the distribution of turbulent dissipation $\varepsilon h/U_*^3$ vs. y/h. The solid line is the semi-theoretical curve which was evaluated from (35) and the mean-eddy scale by Nezu (1977), and it is given by

$$\frac{\varepsilon h}{U_*^3} = 9.76 \frac{\exp(-3 \cdot y/h)}{\sqrt{y/h}} \tag{36}$$

(36) is also valid in the outer region of $y/h > 0.15$. The best agreement between the calculated values and (36) is recognized again in the case of Run 3. Especially, it should be noted that the calculated values coincide well with (36) even near the free surface. This fact indicates that the Hossain free-surface condition of (31) is inadequate.

To sum up, the coefficient C_μ should be described by a van Driest-type damping function. By comparison with semi-theoretical curves, the model constants were reasonably evaluated as $D_1 = 0.95$ and $D_2 = 250$. These values are used in the following discussions.

4.3 Modelling of Damping Effect of Turbulence due to Free Surface

(1) Formulation of Modelling

Although the symmetrical condition of (28) is surely relevant to closed channel flows, its condition cannot be applicable to open-channel flows because the damping effect of turbulence appears near the free surface, as has been pointed out by Nakagawa, Nezu & Ueda (1975). This fact motivated Celik & Rodi (1984) to formulate an algebraic-stress version of the k-ε model. However, this model is very complicated to interpret (29) and (30) physically. Especially, the value of C_μ by using (30) indicated a drastic decrease as the free surface was approached, in spite of the large turbulence-Reynolds-number.

The present modelling is made more straightforward and phenomenologically in the following aspects. The turbulent energy at the symmetrical axis of closed channel flows is defined as k_a, while the turbulent energy at the free surface of open-channel flows is defined as k_w (The axis of the closed channel denotes the suffix a, while its corresponding water surface of the open-channel denotes the suffix w.). The damping effect of turbulence due to the free surface can be described as

$$k_w = D_w \cdot k_a \tag{37}$$

where, D_w is the damping factor. Although it may be difficult to determine the value of D_w theoretically, the following relation is satisfied:

$$D_w = k_w / k_a = \left(\frac{u'_w}{u'_a} \right)^2 \frac{1+(v'/u')_w^2 + (w'/u')_w^2}{1+(v'/u')_a^2 + (w'/u')_a^2} \tag{38}$$

The isotropy of turbulence intensities is nearly satisfied, i. e. $u'_a \simeq v'_a \simeq w'_a$ at the symmetrical axis of closed channel flows (Laufer (1954)). Assuming that $u'_w \simeq u'_a \simeq w'_w$ and $v'_w \to 0$ due to the damping effect of turbulence (Nakagawa et al. (1975) and Ueda et al. (1977)), (38) can be reduced to

$$D_w \to 2/3 \tag{39}$$

Next, the damping effect of turbulence influences the boundary condition of the mean velocity U_w. On the other hand, the Reynolds stress $-(\overline{uv})_w$ should not be influenced by the damping effect because it must obey the Equation (1), i. e. the linear distribution.

Consequently, since $-(\overline{uv})_w = -(\overline{uv})_a$,

$$\frac{dU}{dy}\Big|_w = \frac{1}{\nu_t} (-\overline{uv})_a \tag{40}.$$

In actual computation, (37) and (40) may be satisfied at the nearest grid point y_w to the free surface. It is quite unknown at present how the damping effect of turbulence appears in the turbulent dissipation. Hence, the present study adopts tentatively the symmetrical condition, i. e. $d\varepsilon/dy \mid_{y_w} = 0$.

(2) Experimental Verification

Figure 5 shows the eddy-viscosity distribution of $\nu_t/(hU_*)$ vs. y/h to examine the damping effect of turbulence, by varying the damping factor D_w from 0.4 to 1.0. The experimental values of the open-channel flows in Figure 5 (a) were obtained by Jobson & Sayre (1970), Ueda et al. (1977) and Nezu & Rodi (1986). Nezu & Rodi have recently carried out open-channel experiments by making use of a high power Laser Doppler anemometer. The eddy-viscosity of a closed channel flow becomes nearly constant as the symmetrical axis, i. e. $y/h = 1$, is approached, as has been pointed out by Quarmby & Quirk (1972). The calculated values with no damping effect of turbulence, i. e. $D_w = 1.0$, coincide well with the experimental ones of pipe flows.

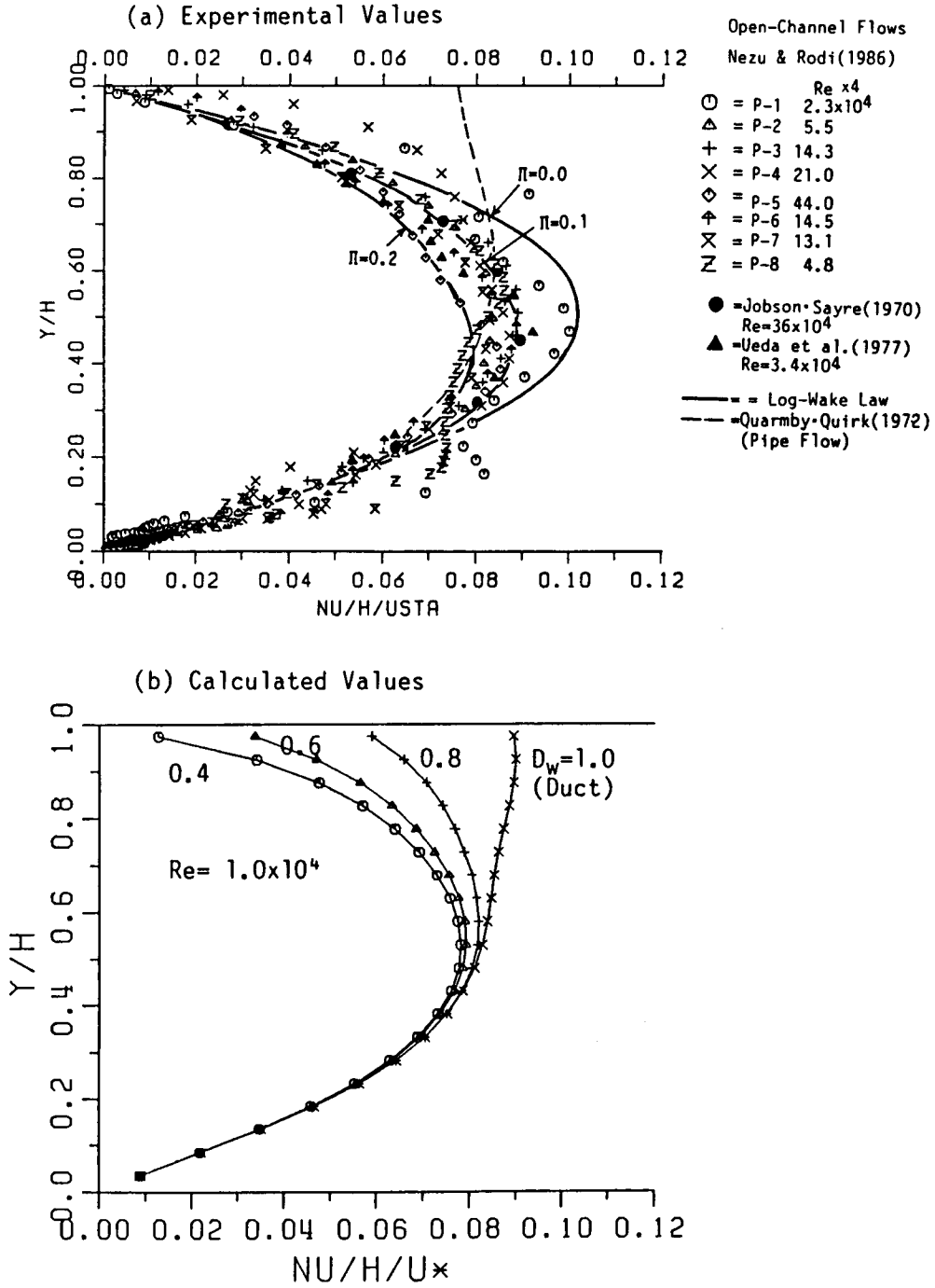

Figure 5. Effect of free-surface damping factor D_w on eddy viscosity distribution, $\nu_t/(hU_*)$.

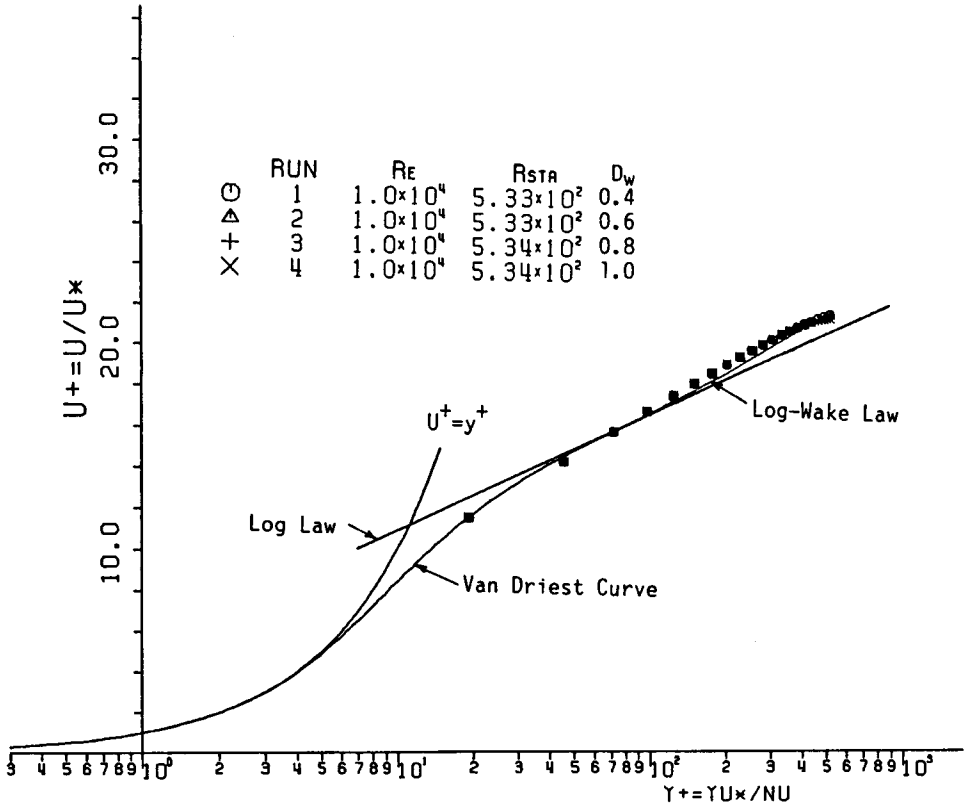

Figure 6. Effect of free-surface damping factor D_w on mean velocity distribution.

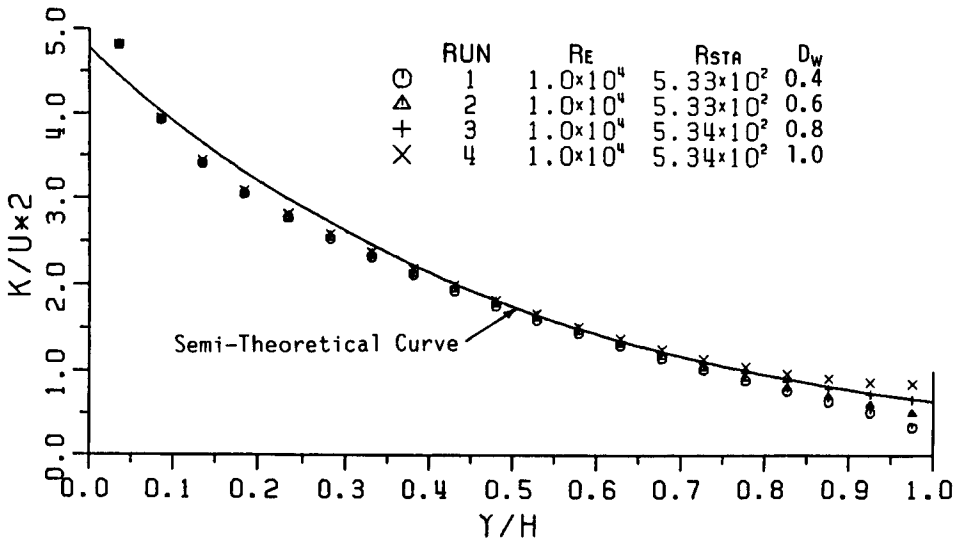

Figure 7. Effect of free-surface damping factor D_w on turbulent energy.

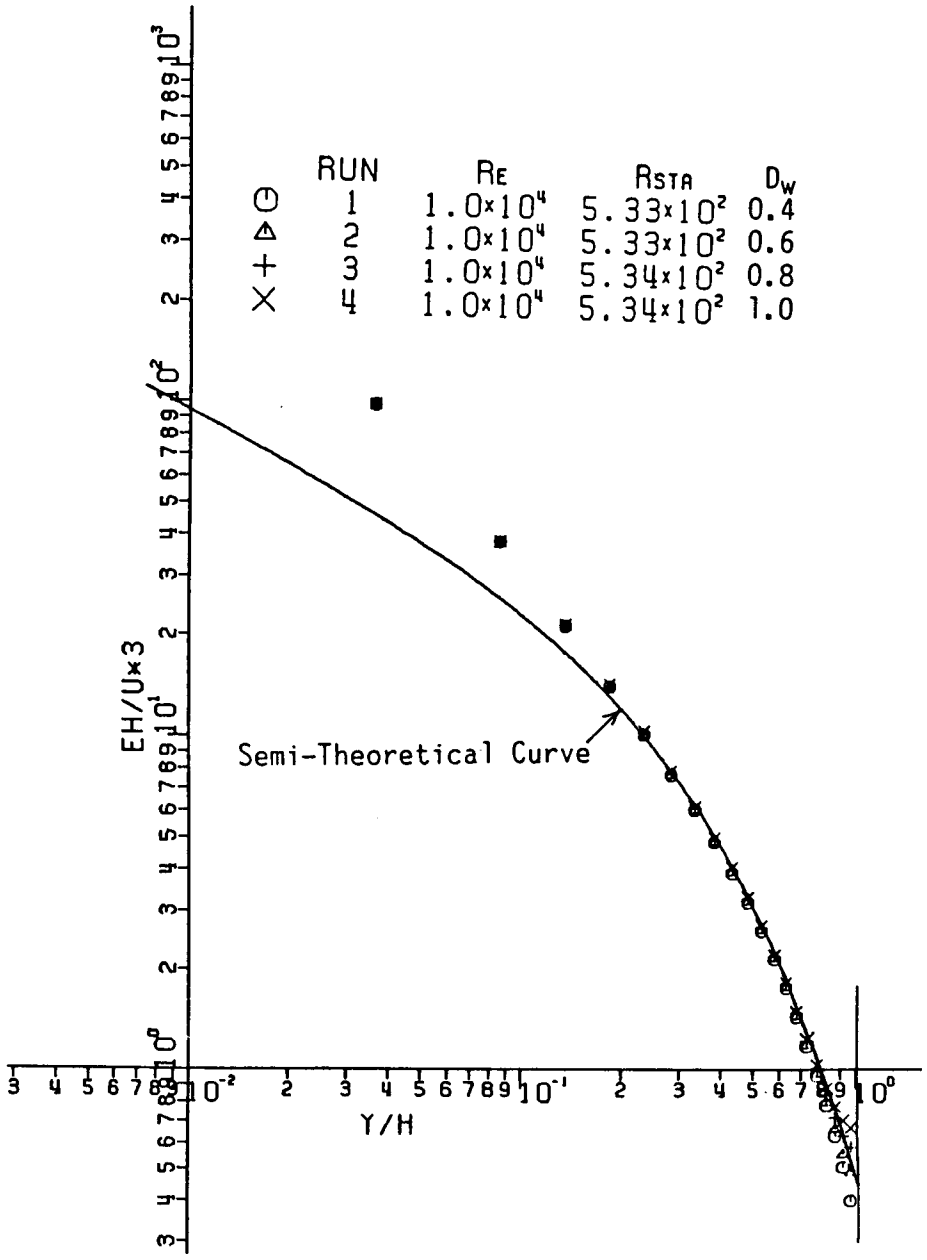

Figure 8. Effect of free-surface damping factor D_w on energy dissipation.

On the other hand, the most noticeable feature is that the eddy-viscosity of open-channel flows decreases as the free surface is approached. This feature can be explained well by introducing the damping factor D_w, as seen in Figure 5 (b). Although the experimental values of ν_t near the free surface are not so accurate because of the numerical difference of the measured mean velocity (Nezu & Rodi (1986)), they may be scattered within the calculated curves of $D_w = 0.4 \sim 0.8$.

Figure 6 shows the mean velocity distributions. The effect of D_w on the mean velocity U^+ is in general small, although a little larger deviation from the log law is recognized near the free surface as the damping factor D_w becomes smaller. The calculated values with $D_w = 0.8$ may coincide well with the log-wake law of (34).

Figure 7 shows the turbulent energy distribution, in which the damping effect of turbulence can be seen clearly near the free surface. The solid line indicates the semi-theoretical curve of (35). In the case of $D_w = 0.8$, the calculated values coincide best with the curve of (35).

Figure 8 shows the turbulent dissipation $\varepsilon h / U_*^3$ vs. y/h, together with the semi-theoretical curve of (36). It is recognized again that the calculated values with $D_w = 0.8$ indicate the best agreement with the curve of (36).

From the above-mentioned results it is concluded that the damping factor can be reasonably determined as $D_w = 0.8$. This value may be plausible in hydraulics, because it is larger than the critical value of $D_w = 0.67$ which is given by a perfect damping, i. e. $v'_w \to 0$.

4.4 Extension of k-ε Model to the Viscous Sublayer

(1) Jones & Launder's extra terms

It is particularly interesting in basic hydraulics to predict the wall region including the viscous sublayer. The reason is that the bursting phenomena occur violently in the region of $y^+ \leq 50$, and thus the turbulent structure does not have equilibrium any longer. Consequently, the turbulent quantities vary rapidly there (e. g. Nakagawa & Nezu (1977, 81)). In this case, Jones & Launder's extra terms D and E should be introduced into the k-ε model, as mentioned in Chapter 2. Although the calculation results by using these extra terms will be shown in Chapter 6, it was found that the coefficient C_μ was the much more essential parameter than the model constants C_3 and C_4 of (11) and (14). C_μ was given by the van Driest-type damping function of (32), i. e. $D_1 = 0.95$ and $D_2 = 250$. From intensive computational optimization in comparison with the experimental results, it was judged that $C_3 = 1.8$ and $C_4 = 2.0$. On the other hand,

Jones & Launder's original data were $C_3 = 2.0$ and $C_4 = 2.0$.

(2) Extension of Wall Function

It is necessary to make a very small finite-difference for the numerical calculation of the wall region of $\delta^+ \equiv \delta U_*/\nu \leq 100$, because the turbulent quantities vary rapidly there. For example, the turbulent energy k and its dissipation ε have maximum values in the buffer layer of $y^+ \leq 30$. However, as the Reynolds number $R_* = hU_*/\nu$ increases, the wall region of $\delta/h \leq 100/R_*$ becomes thinner. Consequently, the number of computational grid points must be increased enormously, which may not be advisable for hydraulic engineering. In order to overcome this difficulty, the minimum position under which the turbulence decreases rapidly, may be chosen as a first grid point, i. e. $y_p^+ = 20$. In the present study, the wall function of the standard model is extended up to $y_p^+ = 20$, as follows:

(i) The mean velocity U_p^+ should be given by the van Driest curve which was obtained from the mixing-length with the viscous damping function.

(ii) Because the turbulent structure becomes non-equilibrium in the region of $y^+ \leq 50$, the equilibrium condition of (25) cannot be used here. However, the following relation may be satisfied.

$$\varepsilon_p = \alpha \cdot G_p \tag{41}$$

where, α is the empirical constant and it can be evaluated from Laufer's (1954) experimental data (See figure 21.) at the initial condition.

From (41) and the van Driest function, the following wall functions can be obtained:

$$k_p/U_*^2 = \frac{1-dU^+/dy^+}{\sqrt{\alpha C_\mu}} \mid y_p^+ \tag{42}$$

$$\varepsilon_p = \frac{C_\mu k^2}{\nu}\left(\frac{dU^+}{dy^+}\right)/\left(1-\frac{dU^+}{dy^+}\right) \mid y_p^+ \tag{43}$$

Setting $dU^+/dy^+ \ll 1$ and $\alpha = 1$, and applying the log law instead of the van Driest curve, (42) and (43) are reduced to the standard wall functions of (26) and (27), respectively.

5. Calculation Results of Open-Channel Flows at High Reynolds Number

5.1 Computational Technique

The turbulent structure of open-channel flows can be calculated by using the present modified k-ϵ model. The hydraulic conditions for high Reynolds numbers are indicated in Table 1. This series is called HR. The Reynolds number $Re \equiv U_m h / \nu$ (where, U_m is the bulk mean velocity) was varied from 2000 up to 10^6. Since the effect of the Froude number $Fr \equiv U_m / \sqrt{gh}$ on turbulence could not be detected, the Froude number was kept constant as $Fr = 0.43$. The first grid point was chosen as $y_p^+ \geq 20$. The staggered grid was adopted here, in which the streamwise grid points were 52 with the grid spacing $\Delta x = h$, and the vertical grid points were 22. The equations of (15) were solved by making use of the modified TEACH code (e. g. Gosman, Launder & Reece (1985)) in which the SIMPLE method of Patankar (1980) was incorporated. The convergence criterion was that the maximum residual of Equation (15) became within

Table 1. Hydraulic conditions for numerical calculation.

(a) High Reynolds-number Series

RUN	h (cm)	U_m (cm/s)	Re $\times 10^3$	Fr	R_*	U_* (cm/s)	$\frac{U_*-U_{*log}}{U_{*log}}$	$\frac{U_*-U_{*wake}}{U_{*wake}}$
HR-1	1.29	15.5	2	0.43	134	1.036	−0.9%	1.8%
HR-2	2.38	21.0	5	0.43	292	1.223	−2.6%	0.08%
HR-3	3.78	26.4	10	0.43	534	1.412	−2.9%	−0.14%
HR-4	11.06	45.2	50	0.43	2,249	2.033	−2.6%	−0.29%
HR-5	17.56	57.0	100	0.43	4,218	2.402	−2.3%	−0.08%
HR-6	81.52	122.7	1,000	0.43	34,545	4.238	−2.3%	−0.35%

(b) Low Reynolds-number Series

LR-1	0.51	9.7	0.5	0.43	38	0.744	−8.8%	−12.1%
LR-2	0.82	12.3	1	0.43	66	0.812	−11.7%	−8.8%
LR-3	1.29	15.5	2	0.43	122	0.943	−9.9%	−7.3%
LR-4	2.38	21.0	5	0.43	274	1.149	−8.5%	−6.0%
LR-5	3.78	26.4	10	0.43	512	1.353	−6.9%	−4.3%
LR-6	11.06	45.2	50	0.43	2,221	2.008	−3.8%	−1.5%
LR-7	17.56	57.0	100	0.43	4,169	2.374	0.4%	−1.2%

U_* = present k-ϵ model,

U_{*log} = from log law, i. e. Eq. (24),

U_{*wake} = from log-wake law, i. e. Eq. (34).

relatively 0.1%. The CPU-time of the numerical calculation for each run was within about one minute by using a large digital computer, FACOM M-382, Data Processing Center, Kyoto University.

Every turbulent quantity approached a definite distribution downstream of $x/h \geq 20$. Hence, the test section was chosen here at $x/h = 42$. In the present calculation, the vertical mean velocity V/U_m was in the same order of magnitude as 10^{-5}, and the mean pressure $P'/(\rho U_m^2)$ was in the order of 10^{-4}. This fact indicates that fully-developed and uniform open-channel flows were obtained at the test section.

5.2 Mean Velocity Distribution

Figure 9 shows the calculation results of mean velocity U^+. For comparison, Figure 10 shows the recent experimental data which were accurately obtained by using Laser Doppler anemometers (Steffler et al. (1985) and Nezu & Rodi (1986)). The calculated values coincide well with the experimental ones in the wall region, including the buffer layer of $y^+ \geq 20$. Nezu & Rodi (1986) have recently emphasized that the mean velocity in the outer region of $y/h \geq 0.15$ deviates, with exact meaning, from the log law in open channel flows as well as boundary layers and closed channel flows. The present calculated values explain

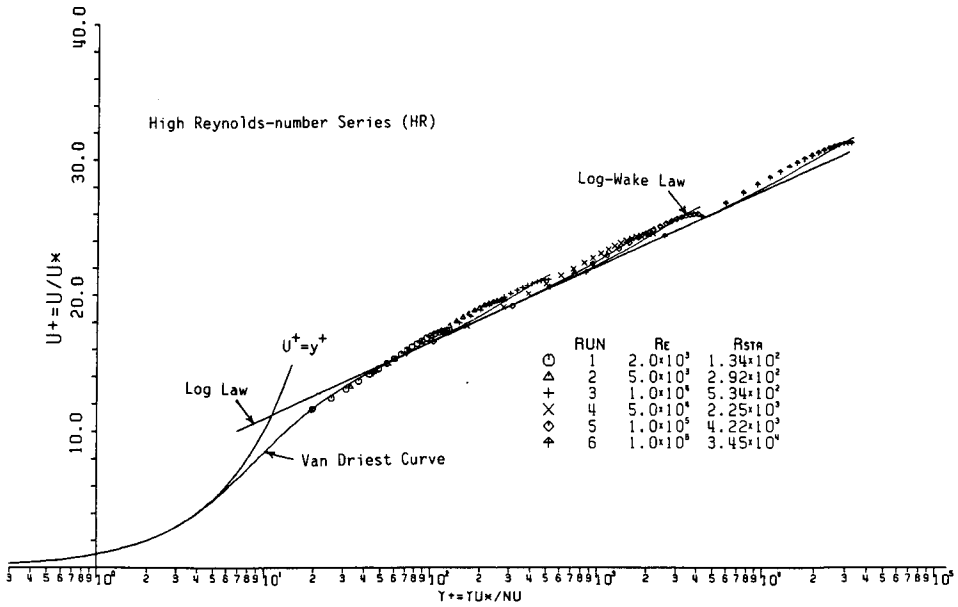

Figure 9. Numerical results of mean velocity distributions for high Reynolds-number series (HR).

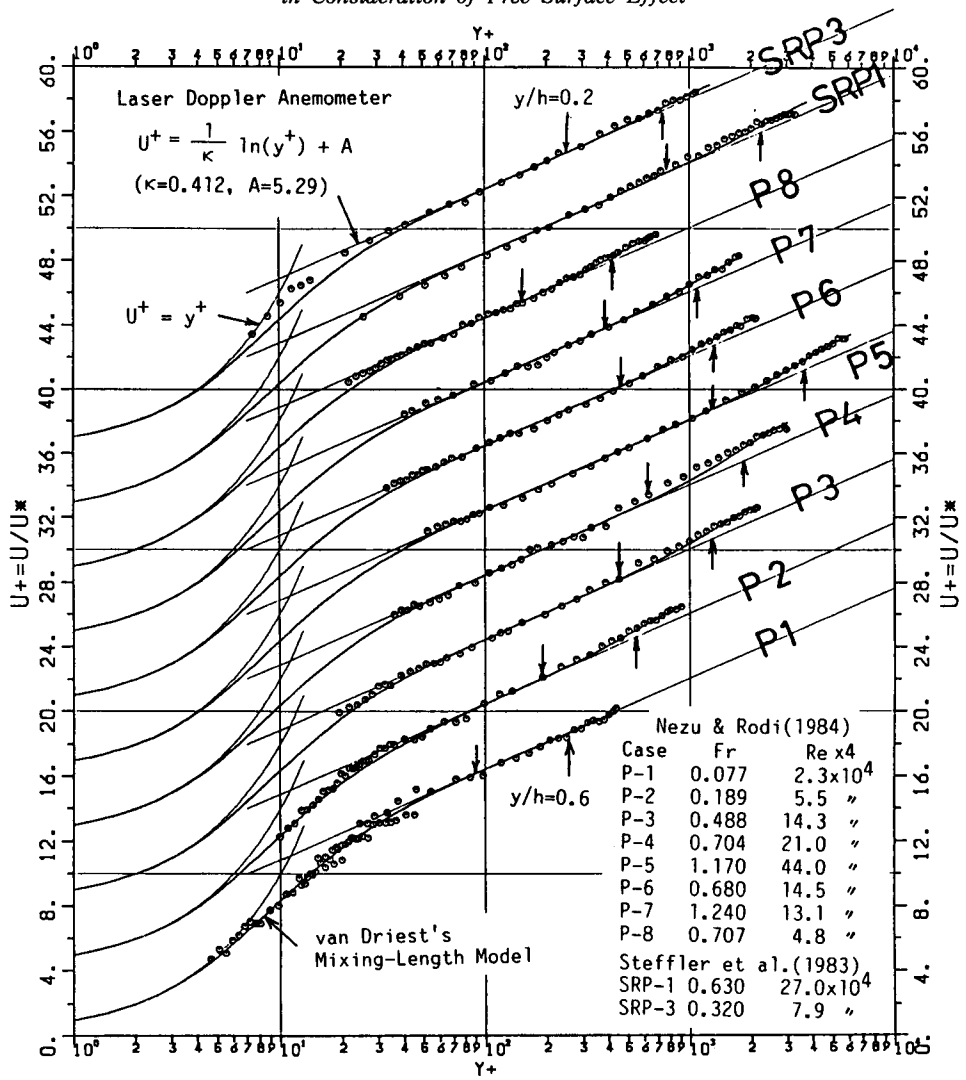

Figure 10. Experimental data of mean velocity distributions by making use of high accurate Laser Doppler anemometers.

well this deviation, which can be described by the log-wake law of (34).

For the purpose of estimating the friction law, the log-wake law of (34) can be applied sufficiently, namely

$$U_m / U_* = \frac{1}{\kappa} \ln (U_* h / \nu) + A + \frac{1}{\kappa} (\Pi - 1) \qquad (44).$$

Of course, when $\Pi = 0$, (44) is reduced to the conventional log law friction.

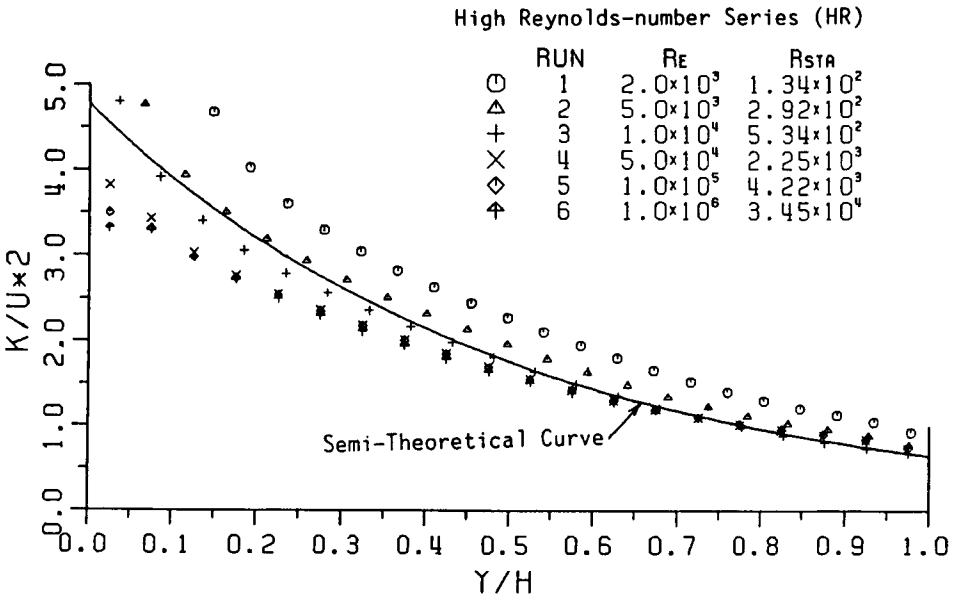

Figure 11. Numerical results of turbulent energy for high Reynolds-number series.

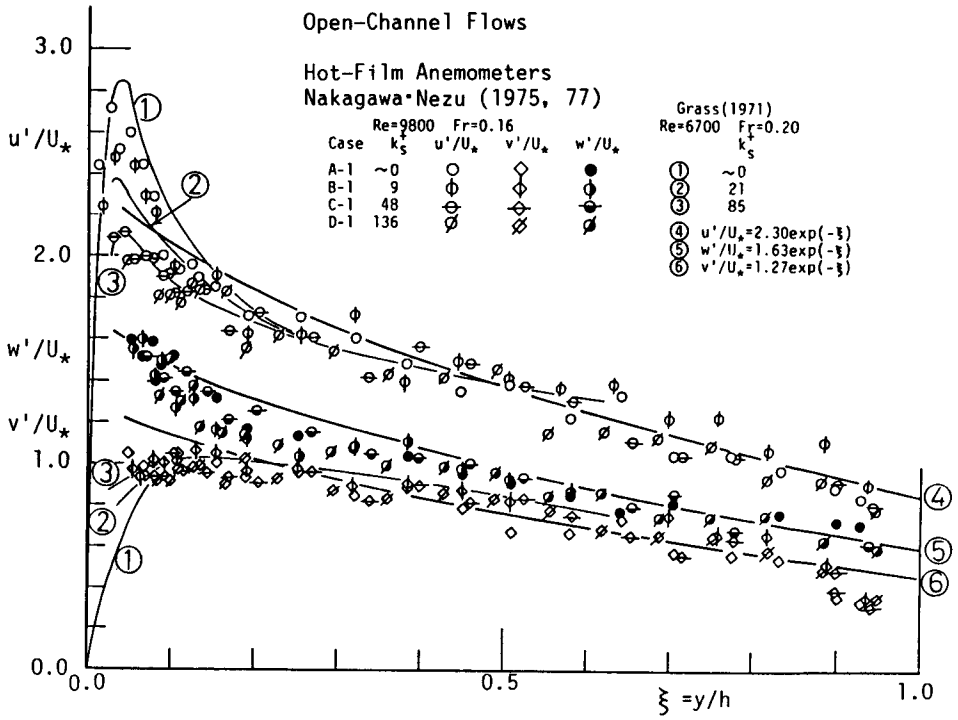

Figure 12. Experimental data of turbulence intensities in open-channel flows by making use of hot-film anemometers (Nakagawa et al. (1975) and Nezu (1977)).

Denoting the friction velocity evaluated from (44) as U_{*log} (log law, i. e. $\Pi = 0$) and U_{*wake} (log-wake law, i. e. $\Pi = 0.2$), a comparison of the calculated values U_* from the present k-ε model is indicated in Table 1. For every run of the HR-series, U_* coincides with U_{*log} within an error of 3%, which may be satisfactory to the prediction in hydraulic engineering. In particular, it should be noted that U_* coincides very well with U_{*wake} within an error of only 0.4%, except for HR-1 which is comparatively low Reynolds number.

5.3 Turbulent Energy and Reynolds Stress

Figure 11 shows the turbulent energy distribution k/U_*^2 vs. y/h. The solid line is the semi-theoretical curve of (35). Figure 12 shows the experimental values of turbulence intensities u', v' and w' which were obtained by using hot-film anemometers (Nakagawa et al. (1975) and Nezu (1977)), and the hydrogen-bubble tracer (Grass (1971)). The turbulent energy k can be easily evaluated as $k = (u'^2 + v'^2 + w'^2)/2$, and be compared with the calculated values in Figure 11. The calculated values at a low Reynolds number, i. e. $Re = 2000$,

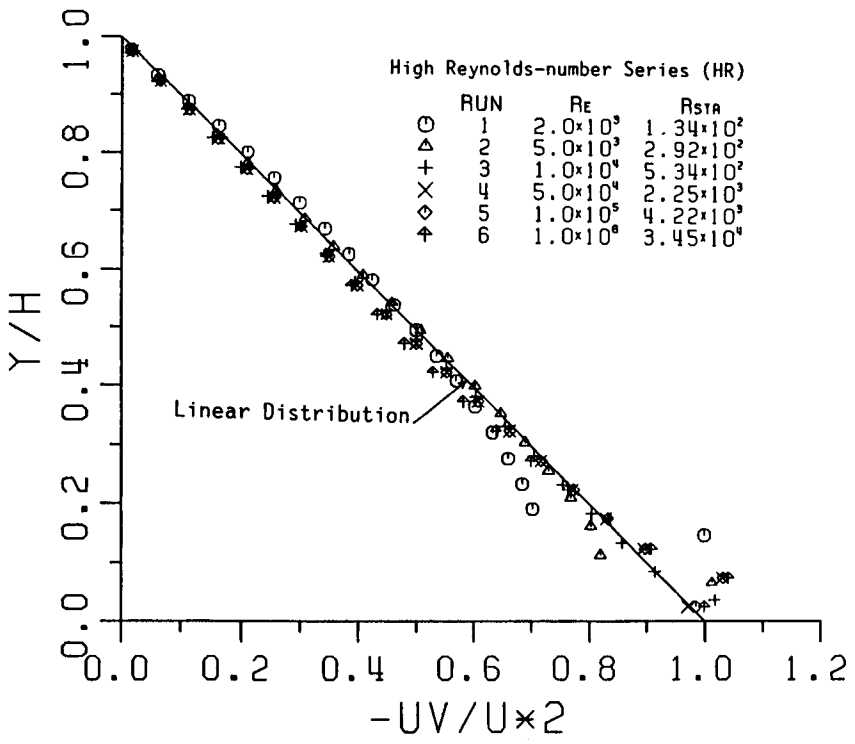

Figure 13. Distribution of Reynolds shear stress.

deviate fairly largely from the semi-theoretical curve of (35) and the experimental values. However, both of them coincide well with each other at high Reynolds numbers of $Re \geq 5000$. Considering the experimental scatter in Figure 12, the present modified k-ϵ model can reasonably predict the turbulent energy in open-channel flows.

Figure 13 shows the Reynolds stress distribution. At a Reynolds number higher than $Re = 5000$, the calculated values of $-\overline{uv}/U_*^2$ obey the linear distribution, which verifies the validity of the present k-ϵ model. In the case of $Re = 2000$, it is, however, impossible to evaluate accurately the velocity gradient near the wall because $y_p^+ = 20$, i. e. $y_p/h = 0.15$ is the first grid point.

5.4 Turbulent Dissipation and Generation

Figure 14 shows the turbulent dissipation $\epsilon h/U_*^3$ vs. y/h. Nezu (1977) evaluated the experimental values of ϵ from the spectral distribution of the u-fluctuations by applying Kolmogoroff's $-5/3$ power law. Although the calculated values at $Re = 2000$ deviate from the semi-theoretical curve of (36), the other runs at higher Reynolds numbers indicate a very good agreement between the observed and calculated values.

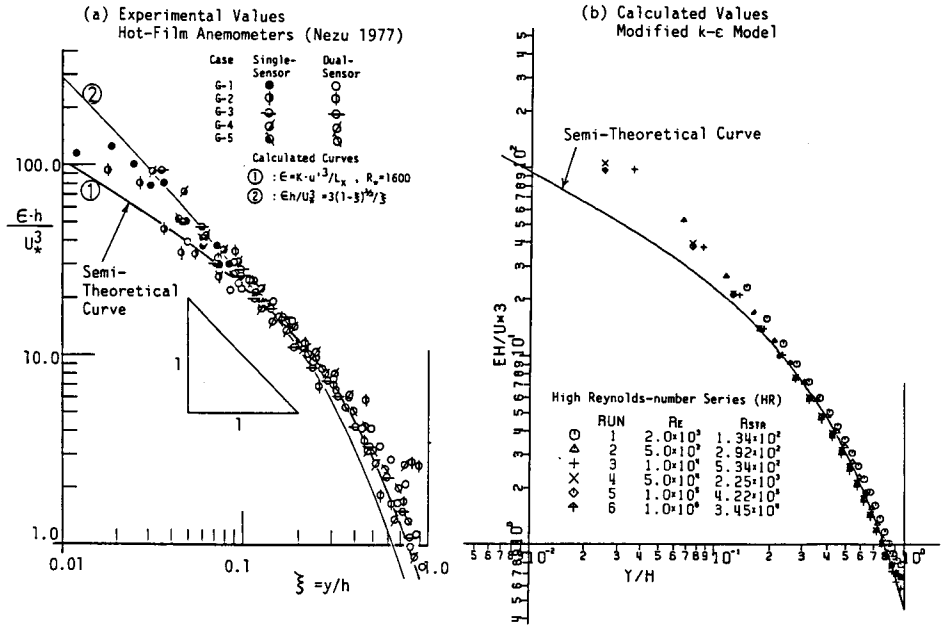

Figure 14. Comparison of calculated values of energy dissipation with experimental ones by Nezu (1977).

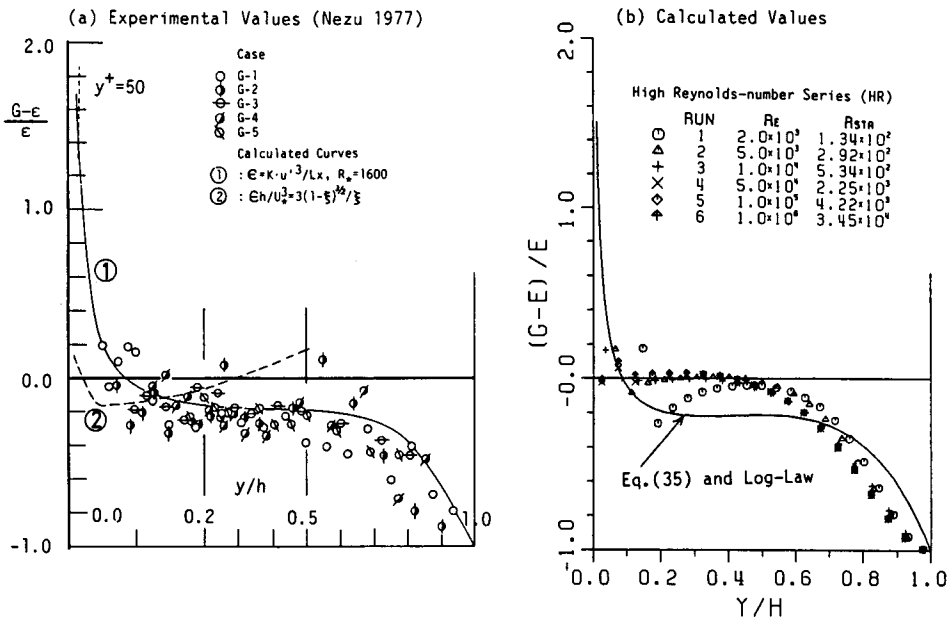

Figure 15. Comparison of calculated values of turbulent generation-dissipation relations with experimental ones by Nezu (1977).

Next, the turbulent generation G can be calculated from (21), and it is plotted as $(G-\varepsilon)/\varepsilon$ in Figure 15. The experimental values of G were evaluated from the numerical difference of the observed mean velocity by Nezu (1977). Except for $Re = 2000$, the calculated values indicate that the equilibrium state of turbulence balance, i. e. $G \cong \varepsilon$, is satisfactory in the region of $0.1 \leq y/h \leq 0.6$. This fact supports numerically the validity of the subdivision of an open-channel flow field by Nakagawa, Nezu & Ueda (1975).

6. Calculation Results of Open-Channel Flows at Low Reynolds Nember

6.1 Computational Technique

The computational technique is basically the same as in Chapter 5. However, in order to divide the grids of the wall region densely, the vertical grid spacing Δy was increased in a geometric ratio, and thus the total number of 52 $\times$ 42 staggered grid points were set in computation. The Reynolds number Re was varied from 500 up to 10^5, as shown in Table 1. The CPU-time was longer than the cases of high Reynolds numbers (HR-series), and it took about 4 minutes for each run.

6.2 Mean Velocity Distribution

Figure 16 shows the mean velocity distribution at a low Reynolds number. It should be noted that the calculated values coincide quite well with the van Driest curve and $U^+ = y^+$ in the viscous sublayer of $y^+ \leq 10$. Accurate experimental data of open channel flows at low Reynolds numbers are not yet available at present, because the experiment control and measurements are quite difficult. Eckelmann (1974) successfully carried out the oil experiments by making use of hot-film anemometers at the low Reynolds numbers of $Re = 2800$ and 4100. He proposed the log law (24) of $\kappa = 0.377$ and $A = 5.9$ in the region of $y^+ \geq 30$, which is replotted in Figure 16. These experimental data coincide well with the calculated ones at $Re < 10^4$. However, one question may occur that the calculated values from the wall-function method for high Reynolds numbers (Figure 9) do not perfectly coincide with the values calculated from the Jones & Launder extra term method for low Reynolds numbers (Figure 16), at the identical Reynolds number. This may not be caused by the shortcomings of the present model itself, but by the difference of the grid spacing between the two methods. The present computational model of open-channel flows for low Reynolds numbers may be satisfactory for $Re \leq 5000$, although a detailed comparison with experimental data will be further necessary.

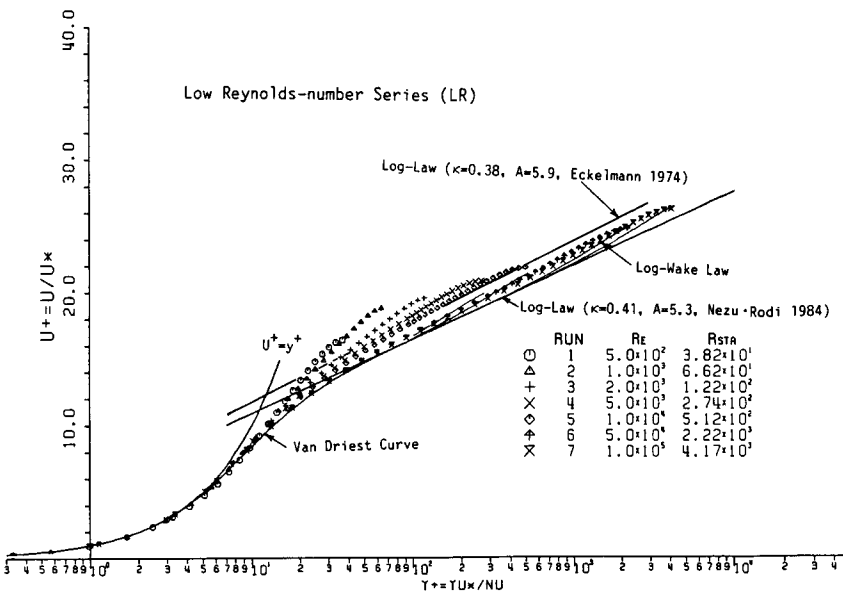

Figure 16. Numerical results of mean velocity distributions for low Reynolds-number series (LR).

6.3 Turbulent Energy and Reynolds Stress in the Wall Region

Figure 17 is the inner-variable description of turbulent energy, i. e. k/U_*^2 vs. y^+. The most noticeable feature is that k/U_*^2 attains the maximum at about $y^+ = 20$, and it becomes flatter as the Reynolds number becomes larger. This maximum value is nearly equal to $k/U_*^2 = 4$, which is in the same order as the experimental values in pipe flows by Laufer (1954). However, after accurate experimental data are available in the wall region, a more detailed examination will be further needed.

A second noticeable feature is that the turbulent energy k decreases more rapidly in comparison with the friction velocity U_*, as the Reynolds number becomes smaller. At $Re = 500$, the maximum value of k becomes only $k = 0.7\ U_*^2$. At this Reynolds number, the mean velocity also deviates from the van Driest curve and approaches the laminar distribution, i. e. $U^+ = y^+$, as shown in Figure 16. Also, the friction velocity U_* indicates a larger deviation from $U_{*\,log}$ and $U_{*\,wake}$ as the Reynolds number becomes smaller, as shown in Table 1. This fact suggests strongly that the open-channel flow may become laminar at a Reynolds number lower than $Re = 500$, which is known empirically in hydraulics.

Figure 18 shows the Reynolds stress distribution in the wall region. As Re becomes larger, the constant-shear-stress layer is surely formed. At $Re = 500$, the maximum value of $-\overline{uv}/U_*^2$ becomes only 0.083, which indicates again the laminar behaviour.

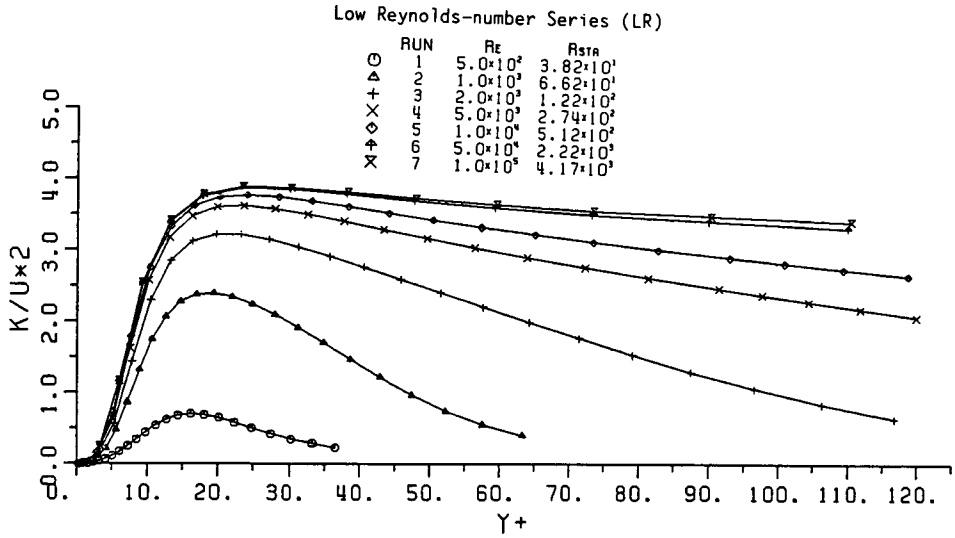

Figure 17. Calculated distribution of turbulent energy in the wall region.

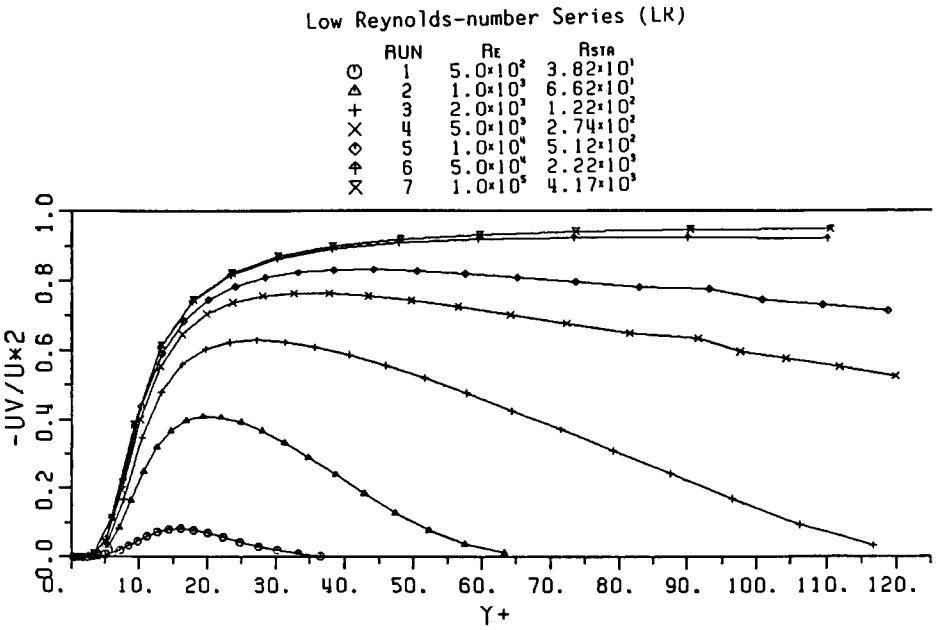

Figure 18. Calculated distribution of Reynolds shear stress in the wall region.

6.4 Turbulent Dissipation and its Generation

Figure 19 shows the outer-variable description of turbulent dissipation, i. e. $\varepsilon h / U_*^3$ vs. y/h. The solid line is the semi-theoretical curve of (36). In the same manner as in Figure 14, a good agreement between the calculated values and (36) is recognized when the Reynolds number becomes larger. The maximum of $\varepsilon h / U_*^3$ becomes larger, and its position also appears closer to the wall as the Reynolds number increases.

On the other hand, Figure 20 is the inner-variable description, i. e. $\varepsilon^+ \equiv \varepsilon\nu / U_*^4$ vs. y^+. ε^+ attains the maximum at $y^+ = 10 \sim 20$, and it indicates universal characteristics as Re becomes larger. These calculated values seem to coincide well with the experimental data of Laufer (1954).

Lastly, Figure 21 shows the ratio $\alpha = G/\varepsilon$ of turbulent generation G to its dissipation ε very near the wall. The calculated values coincide well with the experimental values of Laufer (1954). From this figure, it is understood that the viscous sublayer of $y^+ \leq 6$ is the dissipation region of the turbulence, i. e. $\varepsilon > G$, while the buffer layer of $y^+ \geq 6$ is the production region of the turbulence, i. e. $G > \varepsilon$. Then, the turbulence attains equilibrium, i. e. $G \cong \varepsilon$ when y^+ is greater than 50. This supports the validity of the standard k-ε model of (25). Another interesting feature is that the calculated values may be described by a universal

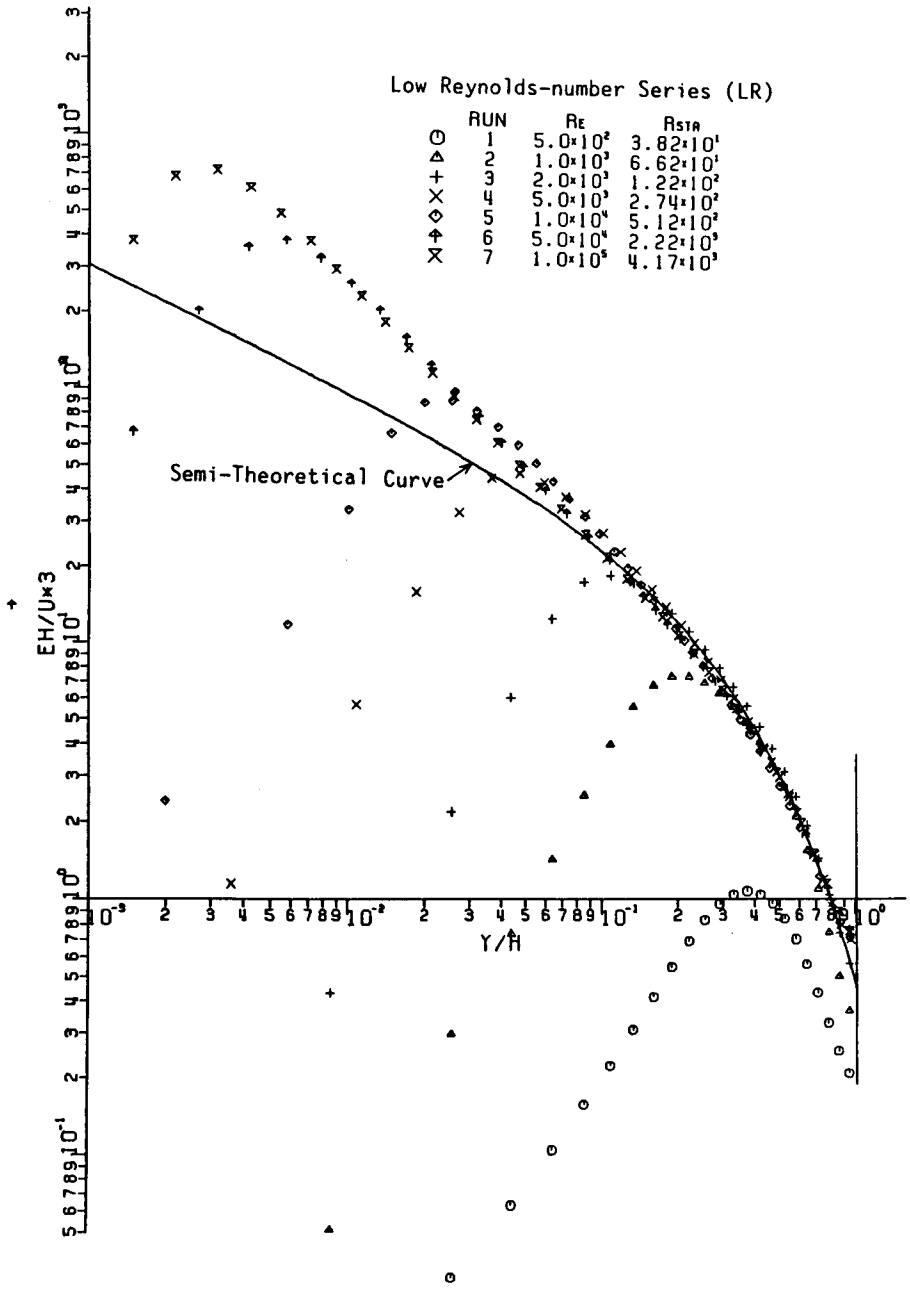

Figure 19. Calculated distribution of energy dissipation (Outer-variable description).

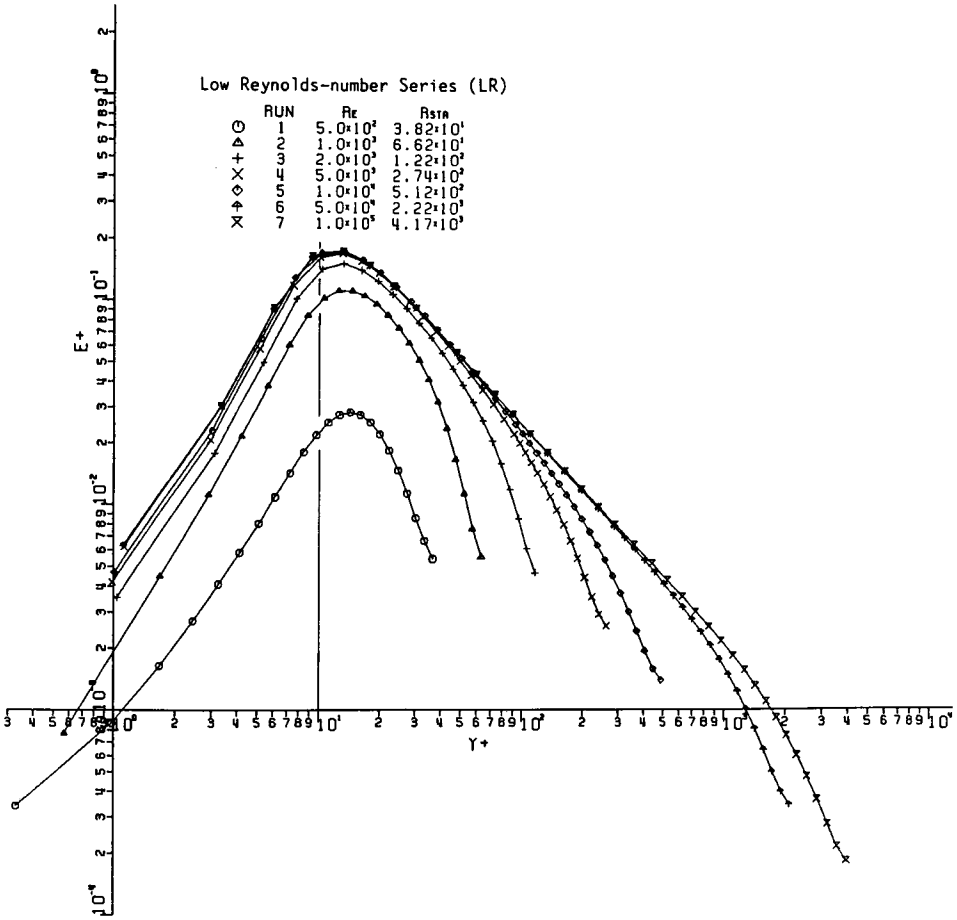

Figure 20. Calculated distribution of energy dissipation (Inner-variable description).

curve even at $Re = 500$. This suggests that, even if the flow is relaminarized, its turbulent structure may be reduced similarly.

7. Conclusions

Numerical calculation techniques of turbulent shear flows are mainly classified as the k–ε turbulence model and the large-eddy simulatiom (LES). The standard k–ε model has been established to predict turbulent structures of jets, boundary layers and closed channel flows in fluid engineering. This is a much more cost-performing computational technique than LES. However, its application to hydraulics, in which the damping effect of turbulence appears near the free surface, is not so available except for Rodi's group. The present study

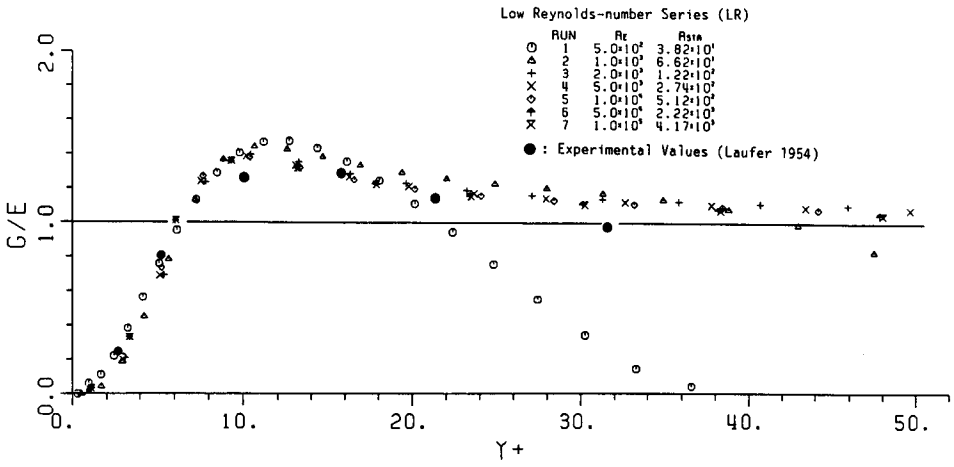

Figure 21. Relation between turbulent generation and dissipation in the wall region.

proposed a new modified k-ϵ model to predict reasonably the turbulent structure of open-channel flows at both low and high Reynolds numbers.

The main modification and extension of the present model are as follows:

(1) The damping effect of turbulence was considered in modelling the free surface condition.

(2) The wall function was extended up to $y^+ = 20$ in order to predict turbulence characteristics near the wall at a high Reynolds number.

(3) The new model was proposed to predict a turbulent structure at a low Reynolds number and, furthermore, in viscous sublayer even at a high Reynolds number.

The present calculation results coincided well with the experimental values of open-channel flows which have been intensively obtained since 1975 by the authors by making use of hot-film and Laser Doppler anemometers.

References

Boussinesq, J. (1877) Essai sur la theorie des eaux courantes. Mem. pres. par div. savants a l'Academie Sci., Paris, Vol. 23, pp. 1-680.

Cantwell, B. J. (1981) Organized motion in turbulent flow. Ann. Rev. Fluid Mech., Vol. 13, pp. 457-515.

Celik, I. & Rodi, W. (1984) Simulation of free-surface effects in turbulent channel flows. Physico-Chemical Hydro., Vol. 5, pp. 217-227.

Deardorff, J. W. (1970) A numerical study of three-dimensional turbulent channel flow at

large Reynolds numbers. J. Fluid Mech., Vol. 41, pp. 453 - 480.

Eckelmann, H. (1974) The structure of the viscous sublayer and the adjacent wall region in a turbulent channel flow. J. Fluid Mech., Vol. 65, pp. 439 - 459.

Gibson, M. M. & Launder, B. E. (1978) Ground effects on pressure fluctuations in the atmospheric boundary layer. J. Fluid Mech., Vol. 86, pp. 491 - 511.

Gosman, A. D., Launder, B. E. & Reece, G. I. (1985) Computer-aided engineering: heat transfer and fluid flow. John Wiley & Sons.

Grass, A. J. (1971) Structural features of turbulent flow over smooth and rough boundaries. J. Fluid Mech. Vol. 50, pp. 233 - 255.

Hanjalic, K. & Launder, B. E. (1976) Contribution towards a Reynolds-stress closure for low -Reynolds-number turbulence. J. Fluid Mech., Vol. 74, pp. 593 - 610.

Hinze, J. O. (1975) Turbulence (2 nd ed.), McGraw-Hill.

Hossain, M. S. (1980) Mathematische Modellierung turbulenter Auftriebs-strömungen. Ph. D. thesis, Univ. of Karlsruhe.

Jobson, H. E. & Sayre, W. W. (1970) Vertical transfer in open channel flow. J. Hydr. Div., ASCE, HY-3, pp. 703 - 724.

Jones, W. P. & Launder, B. E. (1973) The calculation of low-Reynolds-number phenomena with a two-equation model of turbulence. Int. J. Heat Mass Transfer, Vol. 16, pp. 1119 - 1130.

Kobayashi, T. & Kano, M. (1986) Large eddy simulation and numerical analysis of turbulent plane Couette flow. J. of Insti. Industrial Sci., Univ. of Tokyo, Vol. 38, pp. 8 - 14 (in Japanese).

Kobayashi, T., Saga, T. & Matsumoto, H. (1985) Computer generation of channel flow with rectangular turbulent promoters. Symp. Fluid Control and Measurement, Tokyo, Pergamon Press, pp. 763 - 768.

Laufer, J. (1954) The structure of turbulence in fully developed pipe flow. N. A. C. A. TR-1174.

Laufer, J. (1975) New trends in experimental turbulence research. Ann. Rev. Fluid Mech., Vol. 7, pp. 307 - 326.

Moin, P. & Kim, J. (1982) Numerical investigation of turbulent channel flow. J. Fluid Mech., Vol. 118, pp. 341 - 377.

Nakagawa, H. & Nezu, I. (1977) Prediction of the contributions to the Reynolds stress from the bursting events in open-channel flows. J. Fluid Mech., Vol. 80, pp. 99 - 128.

Nakagawa, H. & Nezu, I. (1981) Structure of space-time correlations of bursting phenomena in an open-channel flow. J. Fluid Mech., Vol. 104, pp. 1 - 43.

Nakagawa, H., Nezu, I. & Ueda, H. (1975) Turbulence of open channel flow over smooth and rough beds. Proc. of Japan Soc. Civil Engrs, No. 241, pp. 155 - 168.

Nakayama, A., Chow, W. L. & Sharma, D. (1983) Calculation of fully developed turbulent flows in ducts of arbitrary cross-section. J. Fluid Mech., Vol. 128, pp. 199 - 217.

Naot, D. & Rodi, W. (1982) Calculation of secondary currents in channel flow. J. Hydr. Div., ASCE, Vol. 108, pp. 948 - 968.

Nezu, I. (1977) Turbulent structure in open-channel flows. Ph. D. thesis, Kyoto University.

Nezu, I. & Rodi, W. (1985) Experimental study on secondary currents in open channel flow, 21 st IAHR Congress, Melbourne, Vol. 2, pp. 115 - 119.

Nezu, I. & Rodi, W. (1986) Open-channel flow measurements with a Laser Doppler anemometer. J. Hydr. Eng., ASCE, No. 20573, Vol. 112, pp. 335-355.

Prandtl, L. (1925) Bericht über Untersuchingen zur ausgebildeten Turbulenz. Z. ang. Math. Mach., Vol. 5, pp. 136-137.

Quarmby, A. & Quirk, R. (1972) Measurements of the radial and tangential eddy diffusivities of heat and mass in turbulent flow in a plane tube. Int. J. Heat Mass Transfer, Vol. 15, pp. 2309-2327.

Rodi, W. (1980) Turbulence models and their application in hydraulics. IAHR-Publication, Delft.

Rodi, W. (1986) Use of advanced turbulence models for calculating the flow and pollutant spreading in rivers. 3rd Int. Symp. River Sedim., Univ. of Mississippi, pp. 1369-1382.

Rotta, J. C. (1972) Turbulente Strömungen, Teubner.

Steffler, P. M., Rajaratnam, N. & Peterson, A. W. (1985) LDA measurements in open channel. J. Hydr. Eng., ASCE, Vol. 111, pp. 119-130.

Townsend, A. A. (1976) The structure of turbulent shear flow (2nd ed.). Cambridge Univ. Press.

Ueda, H., Möller, R., Komori, S. & Mizushina, T. (1977) Eddy diffusivity near the free surface of open channel flow, Int. J. Heat Mass Transfer, Vol. 20, pp. 1127-1136.

van Driest, E. R. (1956) On turbulent flow near a wall. J. Aeron. Sci., Vol. 23, pp. 1007-1011.

Willmarth, W. W. (1975) Structure of turbulence in boundary layers. Adv. Appl. Mech. Vol. 15, pp. 159-254.